



Pkd2 Affects Cilia Length and Impacts LR Flow Dynamics and *Dand5*

Raquel Jacinto[†], Pedro Sampaio[†], Mónica Roxo-Rosa, Sara Pestana and Susana S. Lopes^{*}

CEDOC, Chronic Diseases Research Center, NOVA Medical School/Faculdade de Ciências Médicas, Universidade NOVA de Lisboa, Lisbon, Portugal

OPEN ACCESS

Edited by:

Takaaki Matsui,
Nara Institute of Science
and Technology (NAIST), Japan

Reviewed by:

Jeffrey Amack,
Upstate Medical University,
United States
Surya Nauli,
University of California, Irvine,
United States

*Correspondence:

Susana S. Lopes
susana.lopes@nms.unl.pt

[†]These authors share first authorship

Specialty section:

This article was submitted to
Cell Adhesion and Migration,
a section of the journal
Frontiers in Cell and Developmental
Biology

Received: 31 October 2020

Accepted: 12 March 2021

Published: 01 April 2021

Citation:

Jacinto R, Sampaio P,
Roxo-Rosa M, Pestana S and
Lopes SS (2021) Pkd2 Affects Cilia
Length and Impacts LR Flow
Dynamics and *Dand5*.
Front. Cell Dev. Biol. 9:624531.
doi: 10.3389/fcell.2021.624531

The left-right (LR) field recognizes the importance of the mechanism involving the calcium permeable channel Polycystin-2. However, whether the early LR symmetry breaking mechanism is exclusively *via* Polycystin-2 has not been tested. For that purpose, we need to be able to isolate the effects of decreasing the levels of Pkd2 protein from any eventual effects on flow dynamics. Here we demonstrate that *curly-up* (*cup*) homozygous mutants have abnormal flow dynamics. In addition, we performed one cell stage Pkd2 knockdowns and LR organizer specific Pkd2 knockdowns and observed that both techniques resulted in shorter cilia length and abnormal flow dynamics. We conclude that Pkd2 reduction leads to LR defects that cannot be assigned exclusively to its putative role in mediating mechanosensation because indirectly, by modifying cell shape or decreasing cilia length, Pkd2 deficit affects LR flow dynamics.

Keywords: left-right, cilia length, Pkd2, zebrafish, *dand5*, flow dynamics

INTRODUCTION

Vertebrates establish left-right (LR) organization of the internal organs during development. This happens by the action of rotating cilia—5 μ m hair-like structures on the surface of cells—in the left-right organizer (LRO) known as the node in mammals and Kupffer's vesicle (KV) in fish (Essner et al., 2005). These motile cilia generate a directional fluid flow from right to left, which leads to asymmetric intracellular calcium (Ca^{2+}) oscillations (*icos*) (Yuan et al., 2015) in the first layers of cells surrounding the KV. Such *icos* were observed mainly on the left side of the KV midplane and were shown to be dependent on the presence of Pkd2 (Polycystin 2). Therefore, predominant left *icos* precede a left-biased asymmetric expression of genes (such as *nodal*, *lefty2*, and *pitx2*) in the lateral plate mesoderm. Subsequently, these genes will lead to asymmetric localization of internal organs.

The cation channel Pkd2 together with the mechanosensor Pkd1 (Polycystin 1) form a complex which, in the kidney, has the ability to sense the urine flow and induce an intracellular Ca^{2+} signal (Nauli et al., 2003). Pkd2 and its new partner Pkd1-like-1 have also been proposed as the mechanosensor-channel complex responsible for sensing the flow in the LROs of mice, medaka, and zebrafish and conveying the information into the adjacent tissues (Field et al., 2011; Kamura et al., 2011; Roxo-Rosa and Lopes, 2019). Despite working as a complex, it has been shown that

decreasing *Pkd2* alone is sufficient for a strong LR randomization both in mice and in zebrafish (Pennekamp et al., 2002; Bisgrove et al., 2005; Schottenfeld et al., 2007; Yoshida et al., 2012).

However, how the flow is “perceived” by the LRO cells, remains controversial and has not been fully demonstrated. One explanation is provided by the “two-cilia hypothesis,” based on the fact that there are two types of cilia in the mouse node cells: one immotile, the sensory type, capable of detecting changes in the flow, and another motile rotating cilia generating the fluid flow movement (McGrath et al., 2003). An important finding was that *Pkd2* absence in perinodal mouse cilia inhibits the usual asymmetric expression of *cerberus-like2* (*cerl2*) on the right side, important for further LR asymmetry (Yoshida et al., 2012). Motile and immotile cilia have also been found in the zebrafish KV (Sampaio et al., 2014). Perhaps more important, an unbalance on the ratio between motile and immotile cilia types leads to flow defects and to laterality problems with various degrees of severity (Tavares et al., 2017): *situs inversus*, a mirror image of the normal *situs* (*situs solitus*) or various abnormal combinations of thoracic and abdominal *situs*—heterotaxy—which is more severe and can even result in early death in humans (Fliegeauf et al., 2007).

One of the advantages of using zebrafish to answer this question is the ability to manipulate cilia in early development and see the impact of each manipulation in LRO architecture, cilia motility, flow pattern, and organ *situs* in the exact same embryo. We previously characterized flow speed inside the KV by following native particles present in this organ (Sampaio et al., 2014). We reported that there is a main spot of faster flow in WT zebrafish in the anterior dorsal region of the LRO (Sampaio et al., 2014; Tavares et al., 2017) and that when this stereotyped flow pattern is perturbed the expression of the first asymmetric gene, *dand5*, becomes affected (Sampaio et al., 2014). As in mouse (Marques et al., 2004; Oki et al., 2009; Nakamura et al., 2012) and *Xenopus* (Schweickert et al., 2010), *dand5* starts to be symmetrically expressed and by a flow dependent process its expression decreases on the left side. This early *dand5* asymmetry is fundamental for generating the left sided *nodal* cascade of gene expression (Gourronc et al., 2007; Hojo et al., 2007; Lopes et al., 2010; Sampaio et al., 2014). Recently, Vick et al. (2018) showed in *Xenopus* that *Pkd2* is upstream of *Foxj1a* and thereby affects cilia motility and LRO flow. In zebrafish, the role of *Pkd2* has not been tested using adequate cilia or detailed flow quantification methods. In this study, we used both *Pkd2* mutants and antisense technology to manipulate *Pkd2* in the whole embryo or specifically in the LRO and investigated whether reducing *Pkd2* levels affected LRO cilia length and motility thereby impacting on flow magnitude and pattern.

RESULTS

LRO Fluid Flow Is Altered in *Cup*^{-/-} Mutants

First, we started by characterizing flow pattern using the zebrafish *pkd2* mutants, the curly up (*cup*) homozygous mutants (Schottenfeld et al., 2007). We previously demonstrated that *cup*^{-/-} embryos still have *Pkd2* protein (Roxo-Rosa et al., 2015).

Through immunostaining, we found *Pkd2* protein present near the basal body and along the pronephric cilia from visually identified curly up tail *cup*^{-/-} mutants at 36 hpf (Roxo-Rosa et al., 2015). Since this mutant can only produce a truncated version of *Pkd2* protein, which is not detected by our immunostainings, it is fair to assume that the functional protein detected must be maternally deposited as reported by Schottenfeld et al. (2007). So, we assume that embryos at KV stage still have *Pkd2*, even if in reduced levels. Knowing this, we set out to investigate the LRO flow speed and pattern of this “reduced *Pkd2*” condition.

In order to evaluate the flow speed, we recorded the native particles inside the KV of multiple embryos at eight somite stage (ss) using high speed videomicroscopy as previously described (Sampaio et al., 2014). We then generated fluid flow heatmaps at 8 ss from the progeny of *cup* heterozygous crosses in a blind assay. After, we let these embryos develop until they presented either a straight tail that identified them as *cup*[±] or *cup*^{+/+} ($n = 8$) or a curly tail that identified them as *cup*^{-/-} ($n = 9$). In this way, we found that flow speed from *cup*^{-/-} mutants was significantly increased. The flow quantification showed that *cup* homozygous mutants had faster flow (Wilcoxon test; p -value < 0.05) while still maintaining a similar spectrum of cilia beat frequencies (Figures 1A,B). The increased flow speed was unexpected and new as it had previously been noted that *pkd2* morphants had no problems in cilia (Bisgrove et al., 2005).

In search for a reason for the difference in fluid flow between siblings and *cup* homozygous mutants, we repeated the experiment in a *cup* mutant line raised in a *foxj1a*:GFP background to allow for visualization of KV cell shape and overall architecture (Figures 1C,D). The confocal images allowed detailed analysis of the midplane KV cells in two dimensions. Midplane was used because previous modeling studies by our lab (Sampaio et al., 2014) showed this plane displays a maximum lumen area and intercepts the flow vortex, being ideal for 2D studies. Results showed that while *cup*^{-/-} mutants still retained the anterior normal cell shape, with length to width ratio (LWR) > 1, the more posterior cells were significantly less wide compared to their siblings, showing a LWR proximate to 1, which indicates square cells (Figure 1E, p -value < 0.05). When analyzed in more detail, we found out that posterior KV cells in *cup*^{-/-} mutants had different length and width compared to those from their siblings (Figure 1F, p -value < 0.05). However, we did not find a difference in the average number of cells between mutants and their siblings (Figure 1G).

Next, we investigated cilia length and motility. To tackle this, we injected a minimal amount of *arl13b-mCherry* mRNA (50 pg) into 1-cell stage *cup* embryos and performed live imaging at 8 ss to measure cilia length in 3D and quantify cilia motility according to motile or immotile. After, embryos were dis-embedded and allowed to grow until they could be identified by the curly up tail phenotype. We saw a significant decrease of cilia length in *cup* mutants (mean of 5.99 μm) compared with *cup* siblings (8.02 μm, Figure 1H, p -value < 0.05). Since it is known that overexpression of *arl13b* leads to an increase on cilia length (Pintado et al., 2017), we also evaluated the impact of overexpressing *arl13b* mRNA in *pkd2* MO and *pkd2*

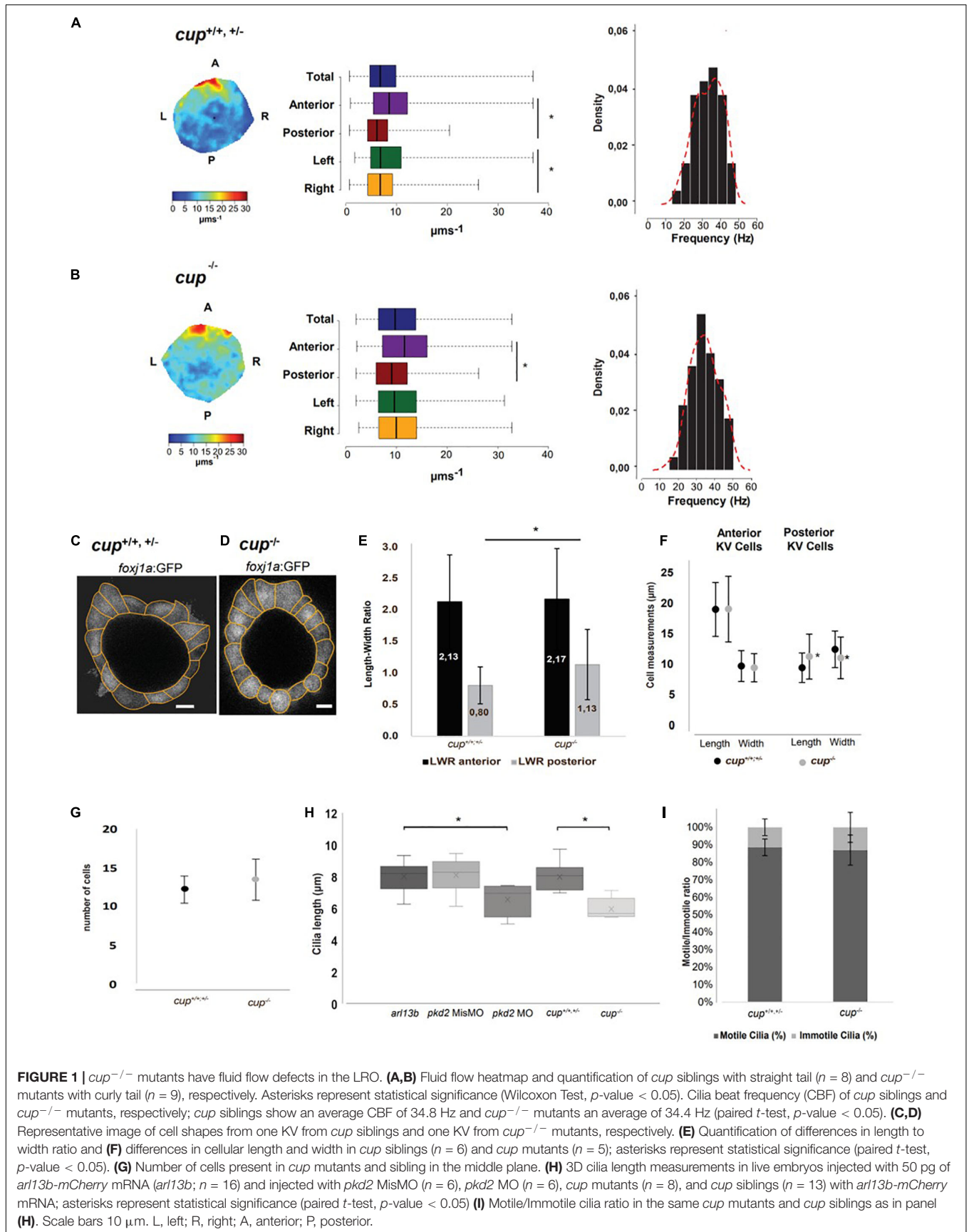


FIGURE 1 | *cup*^{-/-} mutants have fluid flow defects in the LRO. **(A,B)** Fluid flow heatmap and quantification of *cup* siblings with straight tail ($n = 8$) and *cup*^{-/-} mutants with curly tail ($n = 9$), respectively. Asterisks represent statistical significance (Wilcoxon Test, p -value < 0.05). Cilia beat frequency (CBF) of *cup* siblings and *cup*^{-/-} mutants, respectively; *cup* siblings show an average CBF of 34.8 Hz and *cup*^{-/-} mutants an average of 34.4 Hz (paired t -test, p -value < 0.05). **(C,D)** Representative image of cell shapes from one KV from *cup* siblings and one KV from *cup*^{-/-} mutants, respectively. **(E)** Quantification of differences in length to width ratio and **(F)** differences in cellular length and width in *cup* siblings ($n = 6$) and *cup* mutants ($n = 5$); asterisks represent statistical significance (paired t -test, p -value < 0.05). **(G)** Number of cells present in *cup* mutants and sibling in the middle plane. **(H)** 3D cilia length measurements in live embryos injected with 50 pg of *arl13b*-mCherry mRNA (*arl13b*; $n = 16$) and injected with *pkd2* MisMO ($n = 6$), *pkd2* MO ($n = 6$), *cup* mutants ($n = 8$), and *cup* siblings ($n = 13$) with *arl13b*-mCherry mRNA; asterisks represent statistical significance (paired t -test, p -value < 0.05) **(I)** Motile/Immotile cilia ratio in the same *cup* mutants and *cup* siblings as in panel **(H)**. Scale bars 10 μm . L, left; R, right; A, anterior; P, posterior.

MisMO injected embryos. Indeed, despite *pkd2* MO embryos were injected with *arl13b-mCherry* they still showed a significant reduction of cilia length while *pkd2* MisMO did not (Figure 1H, p -value < 0.05). Subsequently, continuing the search for an explanation for the increased flow speed in *cup* mutants we evaluated cilia motility and found that there was no significant difference in the motile to immotile ratio between *cup* siblings and mutants (Figure 1I).

In sum, differences in cell morphology found in *cup* mutants might affect the spacing between posterior KV cilia. However, more experiments should be done to further understand this phenomenon.

LRO Targeted Pkd2 Knockdown Presents Slower Flow and Normal Fluid Flow Pattern

Since we wanted a better approach for Pkd2 removal, we next proceeded by knocking down *pkd2* by means of using an antisense morpholino oligonucleotide (MO), a method that better reduces Pkd2 levels in cilia (Roxo-Rosa et al., 2015) similarly to the PKD2 cilia deprived mouse model (Walker et al., 2019). However, we were already aware that blocking Pkd2 with this morpholino resulted in severely enlarged KVs, with architectural issues (Roxo-Rosa et al., 2015). Also, since it has already been reported that Pkd2 is present in many tissues, including notochord (Mangos et al., 2010), which in turn has been shown to play an important role in KV architecture (Compagnon et al., 2014), we decided to inject the *pkd2* MO in a later developmental stage and specifically target the precursors of the KV—the dorsal forerunner cells (DFCs) (Essner et al., 2005). By co-injecting the *pkd2* MO with the lineage tracer rhodamine-dextran, we could later select the embryos that only showed fluorescence in the yolk cell and the KV (Figure 2A). Below we shall refer to these embryos as *pkd2* MO^{DFCs}.

Our first concern was to evaluate how strong was the Pkd2 knockdown with this DFCs approach. Unfortunately, even increasing the concentration of morpholino injected into DFCs, we were never able to completely remove Pkd2 from KV cilia (Figure 2B). Our second concern was to check if KV architecture was still compromised as in *cup*^{-/-} mutants. At first glance, *pkd2* MO^{DFCs} had a morphologically normal KV when compared with WT (Figure 2C). This was confirmed by measuring the Length-Width ratio of KV cells, which was similar in WT and *pkd2* MO^{DFCs} (Figure 2D). This indicates that cells in the anterior part of the KV are preferentially taller making them more tightly packed together (LWR > 1), while cells in the posterior part are flatter (LWR < 1). This creates an asymmetry of cilia distribution across the anterior-posterior axis of the KV (60–40%), originating the anterior dorsal cluster—an important cilia cluster that creates the anterior flow hotspot (Wang et al., 2011, 2012). So, the asymmetry of cilia distribution is only lost in *pkd2* MO due to the significant architecture alterations the KV suffers from lack of Pkd2 (Figure 2E). The recovery of the architecture with the DFCs-targeted injection of *pkd2* MO shows a typical 60–40% distribution as seen in WT embryos (Figure 2E). Looking more carefully into KV architecture, we

found a significant decrease in cell height between WT and embryos injected with 4 ng of *pkd2* MO^{DFCs} (Figure 2F; p -value < 0.05).

We then checked flow quantification and found that embryos injected with *pkd2* MO^{DFCs} had significant differences between anterior/posterior and left/right KV regions (Figure 2H), as in WT embryos (Figure 2G). These characteristics generated a heterogeneous flow map with a pattern similar to what is found in WT controls. However, total flow speed was slower compared to WT controls (Figure 2G WT 10 μms^{-1} vs. Figure 2H *pkd2* MO^{DFCs} 5 μms^{-1} , p -value < 0.05), indicating that something else other than architecture, which was mostly unchanged, was impacting on flow speed. We also evaluated flow pattern in *pkd2* MO injected at 1 cell stage embryos and, as expected due to KV architectural problems already described by our lab, flow pattern was highly homogeneous (Figure 2I) and also very slow (Figure 2I, *pkd2* MO 4 μms^{-1} , p -value < 0.05). It also had a significantly slower cilia beat frequency (32 Hz compared with WT 34 Hz, p -value < 0.05). Next, we tested for cilia length upon *pkd2* manipulation. Our results clearly showed that cilia length was shorter compared to the controls, either for injections of *pkd2* MO at 1-cell stage or for *pkd2* MO^{DFCs} (Figure 2J, p -value < 0.05). A partial rescue was obtained by injecting 1,000 pg of *pkd2* mRNA (Figure 2J, p -value < 0.05). Cilia length, this time measured in fixed samples without *arl13b* OE was evaluated by anti-acetylated alpha-tubulin staining explaining the general lower values in Figure 2J compared to Figure 1H. We next evaluated cilia motility and found a significant reduction of cilia motility in *pkd2* morphants (Figure 2K, p -value < 0.05), which was also rescued by the injection of *pkd2* mRNA.

In sum, *pkd2* MO impacted extensively on KV architecture, reduced cilia length and motility, which resulted in a slow and homogenous flow. DFCs-targeted injection of *pkd2* MO was less disruptive for KV architecture, but still impacted on cilia length. The resulting flow was heterogeneous but significantly slowed.

Impairment of Pkd2 and Fluid Flow Similarly Affect *dand5* Expression Pattern and Organ Situs

In this new comparative experiment, we used two readouts: (a) *dand5* expression, a nodal inhibitor known to be the first asymmetric expressed gene during the LR axis establishment and (b) internal organ *situs*. In WT zebrafish embryos, *dand5* is mainly expressed on the right side from eight somite stage onward (Lopes et al., 2010; Figure 3A). Our results showed that both manipulations of Pkd2 (whole-embryo and DFCs-injected) lead to *dand5* becoming predominantly symmetric (Figures 3B,C). Similarly, when flow is abrogated by rendering all cilia immotile (*dnah7* MO) (as in Sampaio et al., 2014), *dand5* also became predominantly symmetric (Figure 3D). This shows that, in terms of expression pattern, *dand5* becomes highly symmetric both when there is “no flow” (67%) and when there is “reduced Pkd2 level” (64%). This fact suggests that a Pkd2-mediated sensing of flow is very important to define *dand5* expression pattern, which in WT may be accomplished

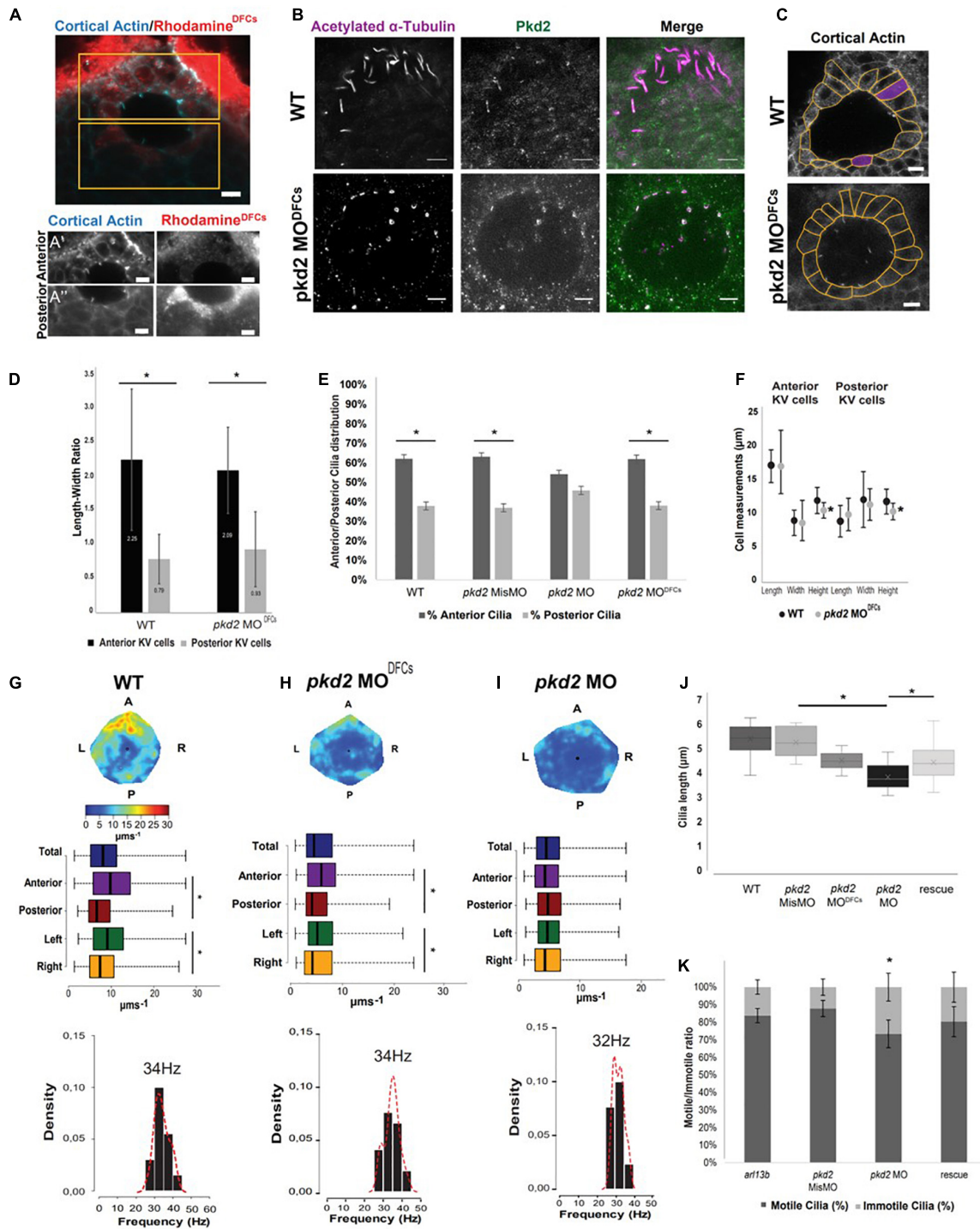


FIGURE 2 | *pkd2* knockdown in the DFCs rescues KV fluid flow pattern. **(A)** Immunostaining for cortical actin and rhodamine showing the result of a successful injection of *pkd2* MO into DFCs, anterior (A') and posterior (A'') panels in the different channels allow for better contrast/brightness balance; **(B)** Immunostaining for Pkd2 in WT and *pkd2*MO^{DFCs} embryos; **(C)** Representative images of KV architecture from one WT embryo and one *pkd2* MO^{DFCs} injected embryo. **(D)** Quantification of the differences in length to width ratio in the KV of WT (*n* = 6) and *pkd2* MO^{DFCs} (*n* = 9). **(E)** Cilia distribution in the antero-posterior axis of the KV of WT embryos (*n* = 22) and embryos injected with *pkd2* MisMO (*n* = 6), *pkd2* MO (*n* = 48) and *pkd2* MO^{DFCs} (*n* = 15). **(F)** Quantification of the differences in cellular length, width, and height, in the same WT and *pkd2* MO^{DFCs} injected embryos from panel **(D)**. **(G–I)** Fluid flow heatmap and quantification of WT (*n* = 8), *pkd2* MO^{DFCs} (*n* = 6) and *pkd2* MO 1-cell stage embryos (*n* = 7), respectively. Asterisks represent statistical significance (Wilcoxon Test, *p*-value < 0.05). **(J)** 3D cilia length measurement in WT (*n* = 23), *pkd2* MisMO (*n* = 8), *pkd2* MO 1-cell stage (*n* = 25), rescue (*n* = 19), and *pkd2* MO^{DFCs} (*n* = 10). **(K)** Motile/Immotile cilia ratio in live embryos injected with *arl13b-mCherry* mRNA (*n* = 8) and injected with *pkd2* MisMO (*n* = 10), *pkd2* MO (*n* = 6) and *pkd2* MO rescued with *Xenopus pkd2* mRNA (*n* = 5). Asterisks represent statistical significance (*p* < 0.05) with paired *t*-test. Scale bars 10 µm. L, left; R, right; A, anterior; P, posterior.

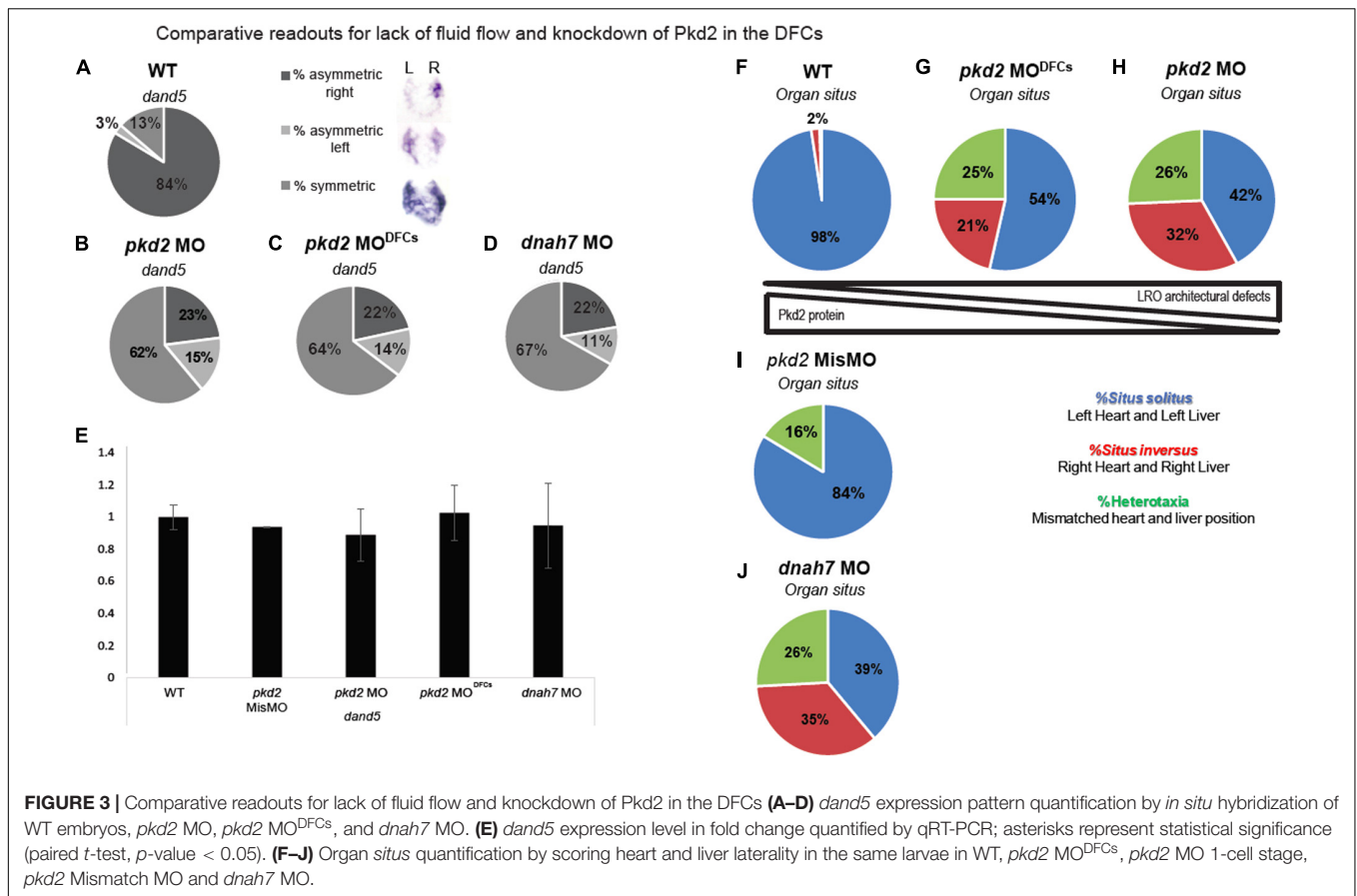


FIGURE 3 | Comparative readouts for lack of fluid flow and knockdown of Pkd2 in the DFCs (A–D) *dand5* expression pattern quantification by *in situ* hybridization of WT embryos, *pkd2* MO, *pkd2* MO^{DFCs}, and *dnah7* MO. (E) *dand5* expression level in fold change quantified by qRT-PCR; asterisks represent statistical significance (paired *t*-test, *p*-value < 0.05). (F–J) *Organ situs* quantification by scoring heart and liver laterality in the same larvae in WT, *pkd2* MO^{DFCs}, *pkd2* MO 1-cell stage, *pkd2* Mismatch MO and *dnah7* MO.

by higher degradation rates of *dand5* mRNA on the left side, where flow is more strongly detected (Oki et al., 2009; Schweickert et al., 2010; Nakamura et al., 2012; Sampaio et al., 2014). As for mRNA expression quantification of *dand5*, qRT-PCRs were performed for each condition. For all treatments there were no differences between WT, *pkd2* MO^{DFCs}, *pkd2* mismatch MO and *dnah7* MO (Figure 3E). This suggests that both impaired flow and manipulation of Pkd2 do not have an impact on *dand5* transcription.

Lastly, we analyzed *organ situs*. Controls showed most cases (97.5%) with left heart and left liver, which means *situs solitus* in zebrafish (Figure 3F). All treatments showed a strong and significant reduction of *situs solitus* when compared to the control situation (Figure 3F) and to the *pkd2* mismatch MO^{DFCs} (Figure 3I) (Fisher test with Bonferroni correction, *p*-value < 0,0125). Both *pkd2* manipulations lead to different amounts of Pkd2 protein being present in the LRO and adjacent tissues, which impacts in LRO architecture and flow pattern/strength defects. However, for LR axis establishment, there seems to be no difference between having “no flow” (Figure 3J) or having defective LRO architecture together with defective flow pattern due to reduced levels of Pkd2 (Figures 3G,H). In sum, *dand5* fails to become asymmetric and *organ situs* becomes randomized between normal (*situs solitus*), a total inversion of *situs* (*situs inversus*) or mismatched combinations of heart and liver position (heterotaxia).

DISCUSSION

In the field of LR axis determination there is increasing evidence for exciting biophysical interactions between extracellular fluid dynamics and cellular sensory mechanisms (Supatto and Vermot, 2011; Yoshida et al., 2012; Sampaio et al., 2014; Smith et al., 2014). With this study we can further confirm that Pkd2 channel plays a major role in the LR axis. Here we use a previously tested antisense morpholino for Pkd2 (Schottenfeld et al., 2007), that effectively reduces Pkd2 levels by antibody staining and leaves only a ring of expression around the base of the cilia (Roxo-Rosa et al., 2015), as described by Walker et al. (2019) for a cilia deprived Pkd2 mouse model. We showed that reducing Pkd2 levels by knockdown experiments decreased cilia length and consequently diminished LRO flow speed, triggering early and late LR defects, as shown by *dand5* symmetric expression pattern and randomized *organ situs*, respectively.

Cilia length was known to greatly affect flow production as the flow produced by an individual cilium scales with the cube of cilia length (Sampaio et al., 2014; Smith et al., 2014). Additionally, we showed here that reduced Pkd2 levels compromised *dand5* mRNA degradation, while its transcription was not quantitatively affected (Figure 3). Furthermore, the differences on *dand5* mRNA patterns between knocking down *dnah7* or *pkd2* were not statistically significant (Figure 3). However, if we could separate the effect of Pkd2 on flow dynamics from its postulated role in

mechanosensation we would predict a different scenario, with near 100% of *dand5* symmetric expression.

As in the *Xenopus* model (Vick et al., 2018) this current study reveals that it is not possible to reduce Pkd2 levels without affecting LRO fluid flow. However, in zebrafish Pkd2 morphants the reasons are different as the number of cilia is not affected (Roxo-Rosa et al., 2015) nor *foxj1a* expression is changed (unpublished data). The reason for the decreased cilia length is not yet understood. However, it is important to disclose this phenotype as it affects the generation of flow. So, comparative studies between animal models within the LR field need to be aware that; 1) Pkd2 in the zebrafish embryo is maternally deposited (Schottenfeld et al., 2007); 2) that even when effectively knocked down, *pkd2* affects other variables, such as cilia length and flow dynamics as well as LRO architecture and fluid volume (Roxo-Rosa et al., 2015), factors that are all crucial in LR early establishment at the LRO level.

We hope this study raises attention to what extent we can use the zebrafish model to study Pkd2 mechanisms, as we do not know the order of events, for example if cell shape changes result from abnormal mechanosensation, or if it is the other way around. In addition, from a slight different angle, we do not know if shorter cilia are a response to cell shape changes or their potential cause.

Regarding the contradictory increase in flow speed scored in *cup* homozygous mutants, we discarded a potential increase in motile cilia or in CBF and confirmed that these mutants also display reduced cilia length. Therefore our data points to cell morphology as the only measured parameter that could cause the referred flow increase. Nevertheless, we cannot assess causality without at least generating appropriate numerical simulations. As to the upstream cause of these differences between mutants and knockdowns we also cannot exclude that the mutation in *cup*^{-/-} mutants, forms a truncated protein that is not degraded and may have undetermined functions and consequences.

Our study intends to alert for some Pkd2 zebrafish facts at the same time it exposes missing causal links. Pkd2 is a central protein in LR development that needs to be studied using conditional mutants with full loss of function in the tissues and in the cilia from those tissues being studied, as reported for the mouse model in some instances (Yoshida et al., 2012; Walker et al., 2019).

Experimental Procedures

Fish Stocks and Genetics

The following zebrafish lines were maintained and used as described elsewhere (Westerfield, 2000): wild-type (AB), *Tg(foxj1a:GFP)* (Caron et al., 2012) and *cup*[±; *Tg(foxj1a:GFP)*]^{tc321}. Embryos were raised at 28 or 32°C, depending on the experiment, in E3 embryo media and staged accordingly (Kimmel et al., 1995). Procedures with zebrafish were approved by the Portuguese DGAV (Direção Geral de Alimentação e Veterinária).

Injections of Morpholino Oligonucleotides

dnah7 morpholino (Sampaio et al., 2014) was diluted in sterile water and injected at one cell stage at a dose of 3 ng per

embryo for *dnah7*. Pkd2 morpholino injection was diluted in sterile water and injected at one cell stage at a dose of 2.5 ng per embryo. To generate chimeric *pkd2* knockdown in DFCs, *pkd2* morpholino (Schottenfeld et al., 2007) was diluted in 10,000 MWt rhodamine-dextran solution (1:4; Sigma-Aldrich) and injected at a dose of 4.2 ng per embryo into the yolk of 512–1,000-cell-stage embryos as previously described (Amack and Yost, 2004). Morpholino injection efficiency was thoroughly controlled as follows: specific *pkd2* MO targeting to DFCs was determined by the rhodamine lineage tracer in KV and yolk cells of the selected embryos (Amack and Yost, 2004; **Figure 2A**); embryos injected with *dnah7* morpholino oligonucleotide were carefully screened by high speed-videomicroscopy for confirming cilia immotility throughout the entire KV. A mismatch *pkd2* morpholino was injected in the same conditions (4.2 ng per embryo) as control. 1,000 pg of *Xenopus pkd2* mRNA was injected at 1 cell stage alone and in combination with *pkd2* MO for rescue experiments. To assess cilia motility and length live, 50 pg of *arl13b-mCherry* mRNA was injected into 1 cell stage embryos.

Live Imaging for Flow Recording

Mounted embryos between 13–14 hpf were set under the 100x/1.30 NA oil immersion objective lens on a Nikon Eclipse Ti-U inverted microscope at room temperature (26°C). All images were taken with the dorsal roof of the KV facing the objective lens. Bright field images were recorded with a FASTCAM MC2camera (Photron Europe, Limited) controlled with PFV (Photron FASTCAM Viewer) software. Native KV particles were filmed at 60 fps for 30 s while cilia were recorded at 500 fps for 2 s. KV flow and CBF measurements were analyzed using Fiji software as described previously (Sampaio et al., 2014). We have successfully analyzed eight WT embryos, nine *cup*^{-/-} embryos, and eight *cup*^{±/±}/*cup*^{+/+} siblings, four *dnah7* MO injected embryos, seven *pkd2* MO 1-cell stage injected embryos and six *pkd2* MO^{DFCs} injected embryos.

Immunofluorescence and *in situ* Hybridization

Whole-mount immunostaining and *in situ* hybridization were performed as described previously (Lopes et al., 2010). Antibodies used for immunostaining were anti-acetylated alpha-tubulin (1:400; Sigma), Alexa Fluor 488 (Invitrogen; 1:500) and Alexa fluor 488 phalloidin (Invitrogen/molecular probes 1:100). Pkd2 immunostaining was performed as described in Roxo-Rosa et al., 2015. Individual *dand5* *in situ* hybridizations were performed at 8–10 somite stage in 37 WT embryos, 13 *pkd2* MO 1-cell stage, 14 *pkd2* MO^{DFCs} and nine *dnah7* MO. *foxa3* *in situ* hybridizations at 53 hpf were performed as described elsewhere (Thisse and Thisse, 2008). Gene expression and *situs* scoring were performed double blind by two investigators and the results were analyzed by Fisher's exact test with Bonferroni correction for multiple comparisons and by Binomial exact test for comparisons in the same genetic background.

Cell Shape and Length-Width Ratio Measurements

Cup[±; *Tg(foxj1a:GFP)*]^{tc321} embryos were mounted live in 2% (w/v) agarose and covered with E3 medium for confocal

epifluorescence microscopy live imaging at room temperature. To assess cell shape, whole KV's were scanned with z sections of 0.5 μm , with an acquisition rate of less than 1 fps. After acquisition, embryos were retrieved from the agarose and let develop for heart scoring and tail phenotype. We imaged 12 *cup*^{-/-} embryos and 19 *cup* sibling embryos. Embryos injected with *pkd2* MO^{DFCs} were immunostained at 14 hpf for actin cytoskeleton and mounted in PBS 1X for confocal epifluorescence microscopy in the same conditions. We imaged 15 *pkd2* MO^{DFCs} injected embryos and 15 siblings from the same fish lines. Selected stacks were subsequently analyzed in Amira for 3D cell shape in KV midplane (five to six embryos for each condition). Results were statistically analyzed by using the paired *t*-test and statistical significance was set at p -value < 0.05.

Cilia Length and Motility

Live embryos were injected at 1 cell stage with 50 pg of *arl13b-mCherry* and then later mounted in 1% (w/v) low-melting agarose at 8 ss, covered in E3 medium. Live imaging was performed in a Zeiss LSM 710 confocal microscope with an Olympus 40 \times water immersion lens (NA 0.8) at room temperature. 3D length of motile and immotile cilia was quantified based on the radial fluorescence intensity profile of each cilium, through semiautomated detection in IMARIS software program (Bitplane, United Kingdom). A total number of 16 *arl13b-mCherry* embryos (291 cilia), six *arl13b-mCherry* + *pkd2* MisMO embryos (92 cilia), six *arl13b-mCherry* + *pkd2* MO (94 cilia), eight *arl13b-mCherry cup* mutants (117 cilia), and 13 *arl13b-mCherry cup* siblings (257 cilia) were measured at 8 ss.

To assess motility, KV's were scanned with z sections of 0.5 μm , with an acquisition rate of 9.6 slices per minute (6.25 s per slice), which provided a pixel dwell time of 22.4 μs . A total number of eight *arl13b-mCherry*, six *arl13b-mCherry* + *pkd2* MO, six *arl13b-mCherry* + *Xenopus pkd2* mRNA + *pkd2* MO (rescue), and 10 *arl13b-mCherry* + *pkd2* MisMO were measured at 8 ss.

Fixed embryos were immunostained with anti-acetylated α -tubulin and imaged in the same confocal. 3D cilia length was measured using the "Simple Neurite Tracer" plugin in Fiji (Longair et al., 2011). A total of 22 WT embryos (1,127 cilia), eight *pkd2* MisMO (497 cilia), 25 *pkd2* MO (1,592 cilia), 19 *pkd2* MO, and *Xenopus pkd2* mRNA (rescue; 996 cilia) and 10 *pkd2* MO^{DFCs} (379 cilia) were measured at 8–10 ss.

Heart and Gut Laterality

At 30 hpf we evaluated heart jogging using a stereoscopic zoom microscope (SMZ745, Nikon Corporation) to observe the embryos from the ventral side. These embryos were then allowed to develop in separated petri dishes and at 53 hpf, embryos were fixed and processed for *foxa3* *in situ* hybridizations to assess gut laterality. We could then pair the heart *situs* with gut *situs* for each treatment and attribute an embryo *situs*. We scored organ *situs* in 159 WT, 31 *dnah7* MO embryos, 140 *pkd2* MO 1-cell stage embryos, 56 *pkd2* MO^{DFCs} embryos and 31 *pkd2* mismatch control-MO injected embryos.

Quantitative PCR

Four groups of ten embryos were used; one group for untreated (control) and the others were injected as explained above and let develop until 8–10 somite stage. After thorough scoring of rhodamin expression only in KV and yolk cell and complete cilia immotility, total RNA was extracted using the Qiagen RNeasy Mini Kit (ref number 74104) and reverse transcribed using both oligo(dT)₁₈ and random hexamer primers with the RevertAid First Strand cDNA Synthesis Kit (ref number K1622) following the manufacturers' instructions. This was repeated three times for three different biological replicates. Expression was quantified by PCR using Roche SYBR Green I Master (reference number 04887352001) and run in a Roche LightCycler[®] 96 Real-Time PCR System. Results were analyzed and depicted as fold-change of transcript levels in injected embryos relative to transcript levels in control embryos. The p -value represents significance in the pairwise comparison of transcript levels between injected and control embryos as determined using the paired *t*-test. Statistical significance was set at p -value < 0.05. *dand5* levels were normalized in relation to *eukaryotic elongation factor 1 alpha 1 like 1 (eef1a1)* and *ribosomal protein L13a (rpl13a)* expression. Primer sequences used were as follows: *dand5* forward 5'-CCGCAATCCTGACCCATAGCAA-3' and reverse 5'-CTCCTCCGTTATGCGCTGTGTA-3'; *eef1a1* forward 5'-CCTTCAAGTACGCCTGGGTGTT-3' and reverse 5'-CACAGCACAGTCAGCCTGAGAA-3'; *rpl13a* forward 5'-TGACAAGAGAAAGCGCATGGTT-3' and reverse 5'-GCCTGTACTTCCAGCCAACTT-3'.

DATA AVAILABILITY STATEMENT

The raw data supporting the conclusions of this article will be made available by the authors, without undue reservation.

ETHICS STATEMENT

The animal study was reviewed and approved by Direção Geral Alimentação e Veterinária.

AUTHOR CONTRIBUTIONS

SL, RJ, and PS conceived and designed the experiments. SL, RJ, and PS analyzed the data and wrote the manuscript. RJ, PS, SP, and MR-R performed the experiments. All authors revised the manuscript.

FUNDING

This work was supported by the Fundação para a Ciência e a Tecnologia (FCT-ANR/BEX-BID/0153/2012 research grant). SL is funded by an FCT CEEC contract for Principal Investigator. The work was also supported by Sociedade Portuguesa de Nefrologia (research grant 2015), iNOVA4Health – UID/Multi/04462/2013 (a program financially supported by Fundação para a Ciência e Tecnologia/Ministério da Educação

e Ciência, through national funds and co-funded by FEDER under the PT2020 Partnership Agreement) and Fundação para a Ciência e Tecnologia (research grant – PTDC/BEX-BID/1411/2014). MR-R was supported by national funds through Fundação para a Ciência e Tecnologia, in the context of the celebration of the program contract foreseen in the numbers 4, 5, and 6 of article 23 of D.L. no. 57/2016 of 29 August, as amended by Law no. 57/2017 of 19 July. Zebrafish used as animal model were reared and maintained in the CEDOC Fish Facility, with the support from the research consortia Congento, co-financed by Lisboa Regional Operational Program (Lisboa2020), under the Portugal 2020 Partnership Agreement, through the European Regional Development Fund (ERDF) and Fundação para a Ciência e Tecnologia

under the project LISBOA-01-0145-FEDER-022170. We also thank the project LysoCil funded by the European Union Horizon 2020 research and innovation under grant agreement No 811087.

ACKNOWLEDGMENTS

The authors would like to thank J. Vermot and L. Saúde for the *cup^{tc321}* mutant and the Tg(*foxj1a*:GFP) zebrafish lines, respectively. We would also like to thank Thomas Johnson-Montenegro, David J Smith, and Bárbara Tavares for their comments and revisions. We would further like to thank the IGC Image and Fish Facilities for great support.

REFERENCES

- Amack, J. D., and Yost, H. J. (2004). The T box transcription factor no tail in ciliated cells controls zebrafish left-right asymmetry. *Curr. Biol.* 14, 685–690. doi: 10.1016/j.cub.2004.04.002
- Biggrove, B. W., Snarr, B. S., Emrazian, A., and Yost, H. J. (2005). Polaris and Polycystin-2 in dorsal forerunner cells and Kupffer's vesicle are required for specification of the zebrafish left-right axis. *Dev. Biol.* 287, 274–288. doi: 10.1016/j.ydbio.2005.08.047
- Caron, A., Xu, X., and Lin, X. (2012). Wnt/beta-catenin signaling directly regulates Foxj1 expression and ciliogenesis in zebrafish Kupffer's vesicle. *Development* 139, 514–524. doi: 10.1242/dev.071746
- Compagnon, J., Barone, V., Rajshekar, S., Kottmeier, R., Pranjic-Ferscha, K., Behrndt, M., et al. (2014). The notochord breaks bilateral symmetry by controlling cell shapes in the zebrafish laterality organ. *Dev. Cell* 31, 774–783. doi: 10.1016/j.devcel.2014.11.003
- Essner, J. J., Amack, J. D., Nyholm, M. K., Harris, E. B., and Yost, H. J. (2005). Kupffer's vesicle is a ciliated organ of asymmetry in the zebrafish embryo that initiates left-right development of the brain, heart and gut. *Development* 132, 1247–1260. doi: 10.1242/dev.01663
- Field, S., Riley, K.-L., Grimes, D. T., Hilton, H., Simon, M., Powles-Glover, N., et al. (2011). Pkd11l1 establishes left-right asymmetry and physically interacts with Pkd2. *Development* 138, 1131–1142. doi: 10.1242/dev.058149
- Fliedrauf, M., Benzing, T., and Omran, H. (2007). When cilia go bad: cilia defects and ciliopathies. *Nat. Rev. Mol. Cell Biol.* 8, 880–893. doi: 10.1038/nrm2278
- Gourronc, F., Ahmad, N., Nedza, N., Eggleston, T., and Rebagliati, M. (2007). Nodal activity around Kupffer's vesicle depends on the T-box transcription factors notail and spadetail and on Notch signaling. *Dev. Dyn.* 236, 2131–2146. doi: 10.1002/dvdy.21249
- Hoyo, M., Takashima, S., Kobayashi, D., Sumeragi, A., Shimada, A., Tsukahara, T., et al. (2007). Right-elevated expression of charon is regulated by fluid flow in medaka Kupffer's vesicle. *Dev. Growth Differ.* 49, 395–405. doi: 10.1111/j.1440-169x.2007.00937.x
- Kamura, K., Kobayashi, D., Uehara, Y., Koshida, S., Iijima, N., Kudo, A., et al. (2011). Pkd11l1 complexes with Pkd2 on motile cilia and functions to establish the left-right axis. *Development* 138, 1121–1129. doi: 10.1242/dev.058271
- Kimmel, C. B., Ballard, W. W., Kimmel, S. R., Ullmann, B., and Schilling, T. F. (1995). Stages of embryonic development of the zebrafish. *Dev. Dyn.* 203, 253–310. doi: 10.1002/aja.1002030302
- Longair, M. H., Baker, D. A., and Armstrong, J. D. (2011). Simple Neurite Tracer: open source software for reconstruction, visualization and analysis of neuronal processes. *Bioinformatics* 27, 2453–2454. doi: 10.1093/bioinformatics/btr390
- Lopes, S. S., Lourenço, R., Pacheco, L., Moreno, N., Kreiling, J., and Saúde, L. (2010). Notch signalling regulates left-right asymmetry through ciliary length control. *Development* 137, 3625–3632. doi: 10.1242/dev.054452
- Mangos, S., Lam, P., Zhao, A., Liu, Y., Mudumana, S., Vasilyev, A., et al. (2010). The ADPKD genes *pkd1a/b* and *pkd2* regulate extracellular matrix formation. *Dis. Model. Mech.* 3, 354–365. doi: 10.1242/dmm.003194
- Marques, S., Borges, A. C., Silva, A. C., Freitas, S., Cordenonsi, M., and Belo, J. A. (2004). The activity of the Nodal antagonist Cerl-2 in the mouse node is required for correct L/R body axis. *Genes Dev.* 18, 2342–2347. doi: 10.1101/gad.306504
- McGrath, J., Somlo, S., Makova, S., Tian, X., and Brueckner, M. (2003). Two populations of node monocilia initiate left-right asymmetry in the mouse. *Cell* 114, 61–73. doi: 10.1016/s0092-8674(03)00511-7
- Nakamura, T., Saito, D., Kawasumi, A., Shinohara, K., Asai, Y., Takaoka, K., et al. (2012). Fluid flow and interlinked feedback loops establish left-right asymmetric decay of Cerl2 mRNA. *Nat. Commun.* 3:1322.
- Nauli, S. M., Alenghat, F. J., Luo, Y., Williams, E., Vassilev, P., Li, X., et al. (2003). Polycystins 1 and 2 mediate mechanosensation in the primary cilium of kidney cells. *Nat. Genet.* 33, 129–137. doi: 10.1038/ng1076
- Oki, S., Kitajima, K., Marques, S., Belo, J. A., Yokoyama, T., Hamada, H., et al. (2009). Reversal of left-right asymmetry induced by aberrant Nodal signaling in the node of mouse embryos. *Development* 136, 3917–3925. doi: 10.1242/dev.039305
- Pennekamp, P., Karcher, C., Fischer, A., Schweickert, A., Skryabin, B., Horst, J., et al. (2002). The ion channel polycystin-2 is required for left-right axis determination in mice. *Curr. Biol.* 12, 938–943. doi: 10.1016/s0960-9822(02)00869-2
- Pintado, P., Sampaio, P., Tavares, B., Montenegro-Johnson, T., Smith, D. J., and Lopes, S. S. (2017). Dynamics of cilia length in left-right development. *R. Soc. Open Sci.* 4, 161102. doi: 10.1098/rsos.161102
- Roxo-Rosa, M., Jacinto, R., Sampaio, P., and Lopes, S. S. (2015). The zebrafish Kupffer's vesicle as a model system for the molecular mechanisms by which the lack of Polycystin-2 leads to stimulation of CFTR. The zebrafish Kupffer's vesicle as a model system for the molecular mechanisms by which the lack of Polycystin-2 leads to stimulation of CFTR. *Bio. Open* 4, 1356–1366. doi: 10.1242/bio.014076
- Roxo-Rosa, M., and Lopes, S. S. (2019). *The Zebrafish Kupffer's Vesicle: A Special Organ in a Model Organism to Study Human Diseases*. London: IntechOpen.
- Sampaio, P., Ferreira, R. R., Guerrero, A., Pintado, P., Tavares, B., Amaro, J., et al. (2014). Left-right organizer flow dynamics: how much cilia activity reliably yields laterality? *Dev. Cell* 29, 716–728. doi: 10.1016/j.devcel.2014.04.030
- Schottenfeld, J., Sullivan-Brown, J., and Burdine, R. D. (2007). Zebrafish curly up encodes a Pkd2 ortholog that restricts left-side-specific expression of southpaw. *Development* 134, 1605–1615. doi: 10.1242/dev.02827
- Schweickert, A., Vick, P., Getwan, M., Weber, T., Schneider, I., Eberhardt, M., et al. (2010). The nodal inhibitor Coco is a critical target of leftward flow in *Xenopus*. *Curr. Biol.* 20, 738–743. doi: 10.1016/j.cub.2010.02.061
- Smith, D., Montenegro-Johnson, T., and Lopes, S. (2014). Organized chaos in Kupffer's vesicle: How a heterogeneous structure achieves consistent left-right patterning. *Bioarchitecture* 4, 119–125. doi: 10.4161/19490992.2014.956593
- Supatto, W., and Vermot, J. (2011). *From Cilia Hydrodynamics to Zebrafish Embryonic Development*. Amsterdam: Elsevier Inc.
- Tavares, B., Jacinto, R., Sampaio, P., Pestana, S., Pinto, A., Vaz, A., et al. (2017). Notch/Her12 signalling modulates motile/immotile cilia ratio downstream of Foxj1a in zebrafish left-right organizer. *eLife* 2017:25165.

- Thisse, C., and Thisse, B. (2008). High-resolution in situ hybridization to whole-mount zebrafish embryos. *Nat. Protoc.* 3, 59–69. doi: 10.1038/nprot.2007.514
- Vick, P., Kreis, J., Schneider, I., Tingler, M., Getwan, M., Thumberger, T., et al. (2018). An Early Function of Polycystin-2 for Left-Right Organizer Induction in *Xenopus*. *iScience* 2, 76–85. doi: 10.1016/j.isci.2018.03.011
- Walker, R. V., Keynton, J. L., Grimes, D. T., Sreekumar, V., Williams, D. J., Esapa, C., et al. (2019). Ciliary exclusion of Polycystin-2 promotes kidney cystogenesis in an autosomal dominant polycystic kidney disease model. *Nat. Commun.* 10:4072.
- Wang, G., Cadwallader, A. B., Jang, D. S., Tsang, M., Yost, H. J., and Amack, J. A. (2011). The Rho Kinase Rock2b establishes anteroposterior asymmetry of the ciliated Kupffer's vesicle in *Zebrafish*. *Development* 138, 45–54. doi: 10.1242/dev.052985
- Wang, G., Manning, M. L., and Amack, J. D. (2012). Regional cell shape changes control form and function of Kupffer's vesicle in the *Zebrafish* embryo. *Dev. Biol.* 370, 52–62. doi: 10.1016/j.ydbio.2012.07.019
- Westerfield, M. (2000). *The Zebrafish Book. A Guide for the Laboratory Use of Zebrafish (Danio rerio)*. Eugene: University of Oregon Press.
- Yoshida, S., Shiratori, H., Kuo, I. Y., Kawasumi, A., Shinohara, K., Nonaka, S., et al. (2012). Cilia at the node of mouse embryos sense fluid flow for left-right determination via Pkd2. *Science* 338, 226–232. doi: 10.1126/science.1222538
- Yuan, S., Zhao, L., Brueckner, M., and Sun, Z. (2015). Intraciliary calcium oscillations initiate vertebrate left-right asymmetry. *Curr. Biol.* 25, 1–12. doi: 10.1007/978-3-540-36348-4_1

Conflict of Interest: The authors declare that the research was conducted in the absence of any commercial or financial relationships that could be construed as a potential conflict of interest.

Copyright © 2021 Jacinto, Sampaio, Roxo-Rosa, Pestana and Lopes. This is an open-access article distributed under the terms of the Creative Commons Attribution License (CC BY). The use, distribution or reproduction in other forums is permitted, provided the original author(s) and the copyright owner(s) are credited and that the original publication in this journal is cited, in accordance with accepted academic practice. No use, distribution or reproduction is permitted which does not comply with these terms.